

An overview of research on wide-speed range waverider configuration

Zhen-tao Zhao¹, Wei Huang^{1*}, Li Yan¹, Yan-guang Yang²

Changsha, Hunan 410073, People's Republic of China

⁵ 2. China Aerodynamics Research and Development Center, Mianyang 621000, China

6

7 **Abstract:** Hypersonic flight is becoming a common development goal of aeronautical and
8 astronautical technology, thus mandating the requirement that hypersonic vehicle have good
9 aerodynamic performance over a wide-speed range. Considering that a waverider is regarded as one
10 of the most promising designs for air-breathing hypersonic vehicles, various design methods of the
11 wide-speed-range hypersonic vehicle based on the design approach of waveriders have been
12 proposed. This paper reviews and classifies wide-speed-range waverider design methodologies
13 developed up until 2019, including the “combined” wide-speed range waverider, the variable Mach
14 number waverider, the vortex lift waverider, the dual/multistage waverider, the morphing waverider,
15 and some other wide-speed-range waverider designs. The current status of the waverider technology
16 is summarized and future development ideas and trends are discussed.

17 **Keywords:** “Combined” wide-speed range waverider; variable Mach number waverider; vortex lift
18 waverider; dual/multistage waverider; morphing waverider

19

20 1. Introduction

The aerodynamic design is a very basic and important part of any aircraft development process,

* Associate Professor, Corresponding author, E-mail: gladrain2001@163.com, Phone: +86 731 84576447

22 because it directly affects the flight performance and flight quality of the entire aircraft, and it has a
23 decisive impact on the flight safety, flight efficiency and economy. At the same time, the
24 aerodynamic design results also directly affect the design of the aircraft structure and of the control
25 system. Küchemann [1] presented a comprehensive review of the aerodynamic design of aircraft
26 which included a chapter on the waverider. In fact, the waverider is a special class of the lifting body
27 aerospace vehicles [2]. Its particularity is that it is a type of vehicle that uses its own shockwave
28 attached to the leading edges to generate extra lift in a high-pressure area below the vehicle to
29 improve its lift-to-drag ratio [3][4]. This characteristic makes it possible to break the ‘L/D barrier’
30 that Küchemann established, which is the great advantage of the special configuration of the
31 waverider [5]. Rodi [6] employed Bezier Curve leading edges to reduce the peak leading edge
32 laminar heating for three waverider-based hypersonic vehicles. At the design Mach number, the
33 waverider “rides” on its shock wave attached to the waverider’s leading edges, the flow between
34 the shock wave and the waverider’s compression-stream surface is fully contained, and there is no
35 spillage from the compression-stream surface to the free-stream surface. This high pressure
36 contained in the flow below the compression-stream surface allows the waverider to have superior
37 aerodynamic performance advantages, such as higher lift-to-drag ratio than conventional,
38 nonwaverider hypersonic configurations. However, at off-design Mach numbers, the shock wave is
39 detached from the waverider’s leading edges and there is flow spillage, which will adversely affect
40 the aerodynamic performance advantages of the waverider. This is also one of the restraints on the
41 practical application of the hypersonic waverider. That is to say, the optimal waverider configuration
42 is highly dependent on Mach number, and a small deviation from the design point may significantly
43 degrade its aerodynamic performance advantages over conventional vehicles [7][8].

Therefore, many researchers [9][10][11][12][13][14] have attempted to make the waverider meet various practical needs, and after decades of development, the waverider configuration has developed into the waverider family of vehicles [15][16][17][18][19][20]. For example, in order to further increase the lift-to-drag ratio of waveriders at useful lift coefficients, the Osculating Cones Method was developed [21][22][23][24]. On this basis, the Osculating Flowfield Method was also proposed. This research showed that waveriders generated with the Osculating Flowfield Method have a higher lift-to-drag ratio than those created using the Osculating Cones Method [25][26][27][28][29][30][31]. In order to ensure that the lift-to-drag ratio and volumetric efficiency of a hypersonic airplane are both at a high level, Cui et al. [32] proposed a type of hypersonic airplane configuration with a double flanking air inlets layout, and Rodi [33] developed an optimization process for the Osculating Flowfield waverider generation method. In order to provide a highly uniform inlet flowfield to a scramjet engine system, the waverider was used as the forebody of the air-breathing hypersonic vehicle [34][35][36][37][38]. Furthermore, in order to take full advantage of the waverider's high lift-to-drag characteristics and the ideal pre-compression surface for the engine, the waverider design was used as the basis for the design of the entire air-breathing hypersonic vehicle [39][40][41][42][43]. At present, faced with the inevitable development target of developing a reusable Aerospace Vehicle (AV) for an Earth/Orbit Space Transportation System, the study of waveriders has also ushered in new development opportunities. Therefore, in order to overcome the technical limitation of the single Mach number waverider configuration, and also to better satisfy the practical requirement of the aerospace vehicle's wider speed range and wider airspace, a variety of novel designs have been proposed.

The main objective of this paper is to summarize the various current design methods for

66 waveriders with a wide-speed range, and to discuss the next development ideas and trends of the
67 wide-speed range waverider. The remainder of this survey is organized as follows. Sections 2-7
68 detail the several types of wide-speed range waverider designs. Section 8 provides a discussion and
69 Section 9 concludes this paper.

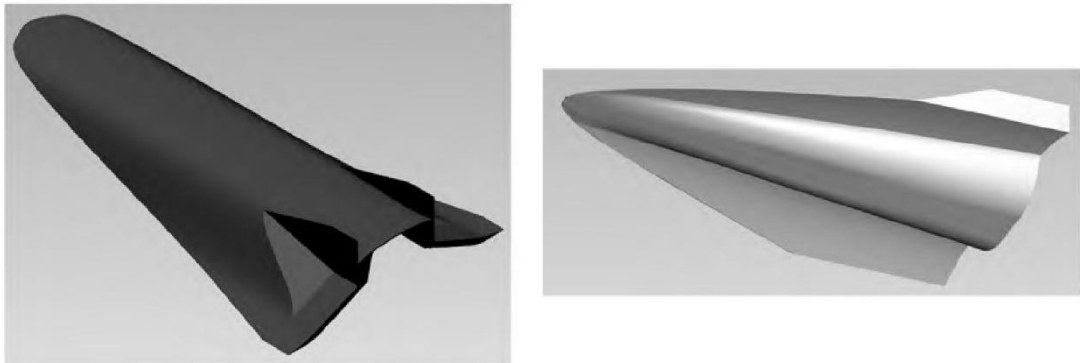
70

71 **2. The “combined” wide-speed range waverider**

72 Just as its name implies, the “combined” wide-speed range waverider is a combination of the
73 waverider generated under different design conditions by splicing either directly or by using the
74 connecting segments. The expected goal of this scheme is to combine two or more waveriders
75 generated under different design conditions to ensure that when the flight Mach number varies
76 within a certain range, a part of the aerodynamic performance of the designed waverider decreases
77 while the other part increases. Therefore, the overall aerodynamic performance of the designed
78 waverider is better under wide-speed flight conditions.

79 In 2009, in order to improve the aerodynamic performance of the waverider in the full-speed
80 range of the flight envelope, Wang et al. [44] put forward a wide-speed range waverider design
81 method by means of combination and stitching. The design schemes are as follows: Firstly, they
82 used the osculating cone theory to design a hypersonic waverider (Mach number $Ma=6.0$, flight
83 height $H=30km$) and a low-speed waverider (Mach number $Ma=3.0$, flight height $H=15km$), and
84 performed an engineering design according to relevant requirements, as shown in Fig. 1. And then,
85 by joining the low-speed waverider and hypersonic waverider with an adapter, a wide-speed range
86 waverider was designed, as shown in Fig. 2. The results of wind tunnel test and numerical simulation
87 show that the maximum lift-to-drag ratio of this wide-speed range waverider is more than 3.5 over

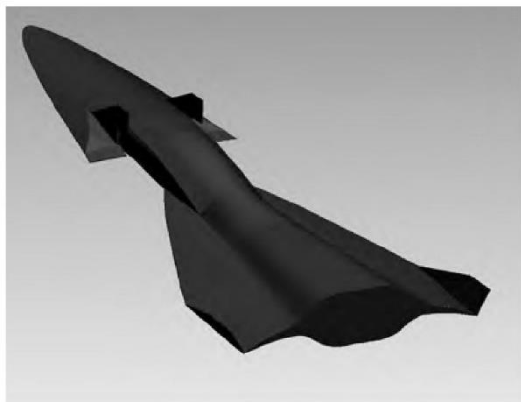
88 the entire flight envelope ($0.3 < Ma < 7.0$), which indicates that it can maintain a good aerodynamic
89 performance in the wide-speed range of subsonic, transonic, supersonic and hypersonic speeds.



(a) The hypersonic waverider configuration (b) The low-speed waverider configuration

90 Fig. 1 The hypersonic and low-speed waverider configurations generated by the osculating cone

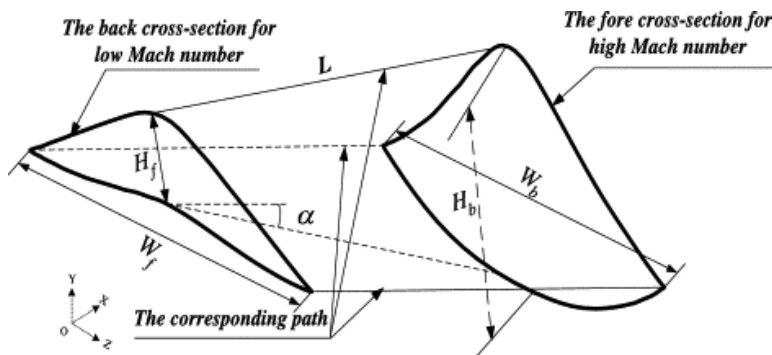
91 theory [44].



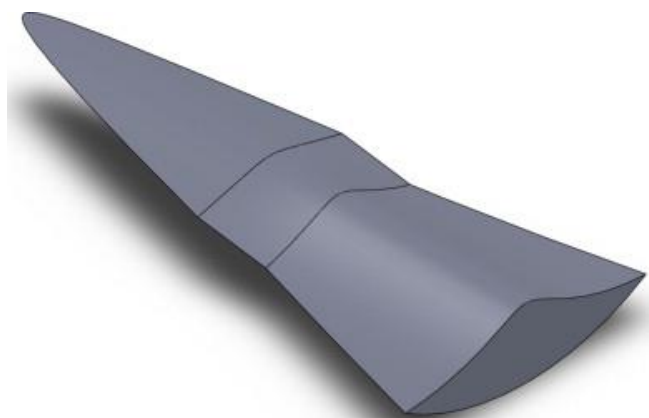
92
93 Fig. 2 The wide-speed range waverider configuration [44].

94 In 2013, in order to study the influence of the connection section on the aerodynamic
95 performance of the "tandem" wide-speed range waverider, Li et al. [45] designed a "tandem" wide-
96 speed range waverider based on the cone-derived theory, as shown in Fig. 3. The effects of the
97 length of the connection section, the thickness of the front body and the width of the rear body on
98 the aerodynamic performance of such a wide-speed range waverider were analyzed by means of the
99 numerical approaches. The obtained results show that the lift-to-drag ratio of the "tandem" wide-
100 speed range waverider is proportional to the length of its connection section, the thickness of its

101 forebody and the width of its afterbody. The length of the connection section has the most obvious
 102 influence on the aerodynamic performance of such an aircraft, and the influence of the width of the
 103 afterbody on its overall aerodynamic performance is not obvious. In addition, the influence of the
 104 forebody's thickness and the connection section's length on the aerodynamic performance of the
 105 aircraft is coupled.



106
 107 (a) Generating principle of the connection section

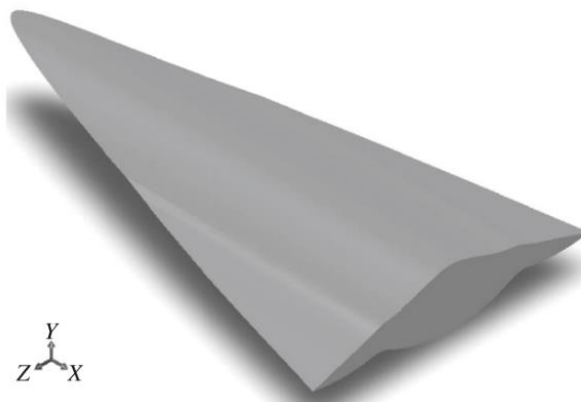


108
 109 (b) The configuration of the "tandem" wide-speed range waverider

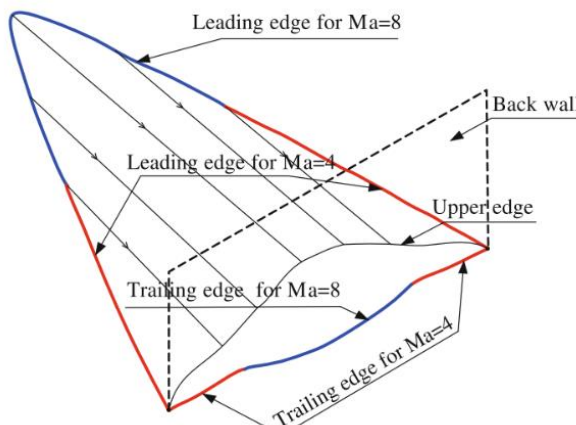
110 Fig. 3 The "tandem" wide-speed range waverider [45].

111 In 2014, inspired by the design method of the "tandem" wide-speed range waverider, and
 112 considering that the shock wave characteristics of the waverider are mainly determined by the shape
 113 of its leading-edges, Li et al. [46] also designed a "parallel" wide-speed range waverider, as shown
 114 in Fig. 4 (a). The idea of the design is to first obtain the leading-edges of the two benchmark models
 115 of the high-Mach and low-Mach waveriders by using the design theory of the cone-derived

116 waverider. Then, the two leading-edges are combined in parallel to obtain the "parallel" wide-speed
 117 range waverider. The generation of its trailing edge is also the same, as shown in Fig. 4 (b). The
 118 numerical results show that compared with the two reference configurations, the "parallel" wide-
 119 speed range waverider has a higher lift-to-drag ratio in the hypersonic speed range, which shows
 120 that the "parallel" design method can improve the overall aerodynamic performance of the
 121 waverider. Moreover, the wide-speed range waverider designed in parallel mainly improves its lift-
 122 to-drag ratio by reducing its flight drag.



123
 124 (a) The configuration of the "parallel" waverider



125
 126 (b) The design theory of the "parallel" waverider

127 Fig. 4 The "parallel" wide-speed range waverider [46].

128 In addition to the above-mentioned design method of combining and splicing two waveriders,

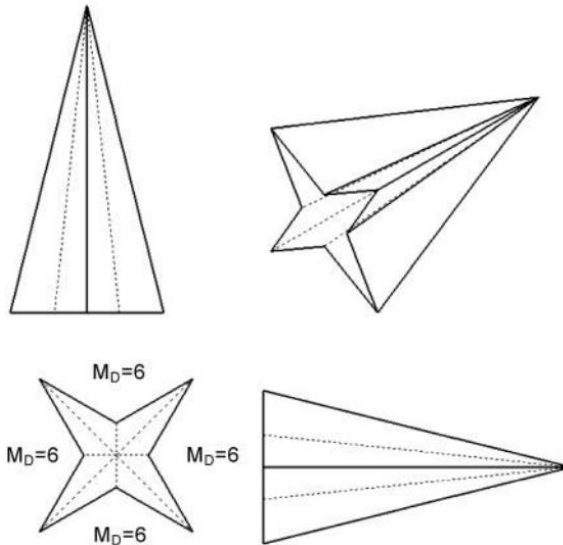
129 it is also possible to combine several waveriders, that is, a kind of design called the star-body
130 waverider. Similar to the star-shaped body, they can be generated by combining a plurality of wedge-
131 derived waveriders, conceived by Nonweiler [47], as shown in Fig. 5. Its advantage is that they have
132 a lower wave drag than the right circular cones with equivalent length and volume [48][49][50].

133 However, because the star-body waverider shown in Fig. 5 is generated for the same design
134 Mach number, the shock wave will no longer attach to the fin leading edges when flying at any
135 Mach number other than the design Mach number, resulting in shock detachment, thus reducing
136 aerodynamic efficiency, which is not conducive to the wide-speed flight of the waverider. In addition,
137 because the wedge sections of the star-shaped body have the same flow deflection angle, such an
138 axisymmetric configuration will only produce a finite aerodynamic drag while flying at zero angle
139 of attack, but will not contribute to the lift or side force. In view of the above problems, Stephen
140 Corda designed a class of star-body waveriders with multiple design Mach numbers by arranging
141 different design Mach numbers for each center wedge section [51], as shown in Fig. 6. It may
142 produce a more optimized aerodynamic configuration “tailoring” over a range of Mach numbers.

143 On this basis, using the computational fluid dynamics method, Corda analyzed the aerodynamic
144 characteristics of a single- and multiple-design-Mach-number star-body waverider. The numerical
145 results show that the single-design-Mach number star-body waverider has higher skin-friction drag,
146 lower wave drag, and lower total drag than the equivalent volume cone. Because the volume and
147 the wetted surface areas of the multiple-design-Mach-number star-body waverider are relatively
148 large, its total drag is higher than that of the equivalent cone, but for some of these new
149 configurations with higher Mach numbers, their wave drag and drag coefficient are lower than that
150 of the equivalent cone. Furthermore, in order to generate lift or side force, the section of the multiple-

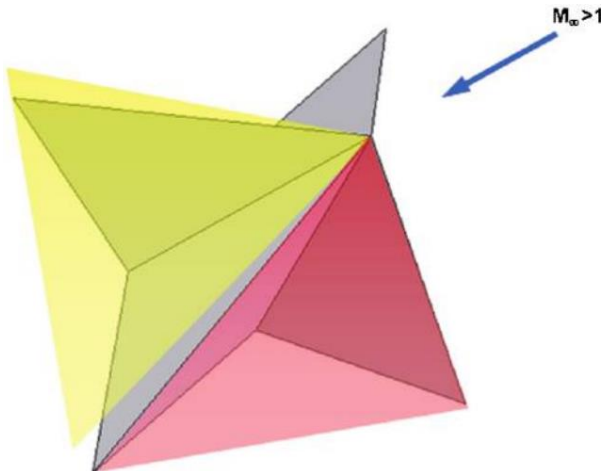
151 design-Mach-number star-body waverider should be designed as follows: the sector with the higher

152 design Mach number should correspond to the desired direction of force.



153

154 Fig. 5 The star-body waverider with one design Mach number, $Ma_D = 6.0$ [47].



155

156 Fig. 6 The multiple-design-Mach-number star-body waverider [51].

157 Among the various design schemes for wide-speed range waveriders proposed at present, the

158 design idea of combination and splicing is undoubtedly the most intuitive. It can be seen from the

159 current research results that the aerodynamic performance of the wide-speed range waverider

160 designed with this idea is superior to the ordinary waverider that constitutes it. However, this design

161 idea is based only on artificially splicing the waverider simply and mechanically. Therefore, it is

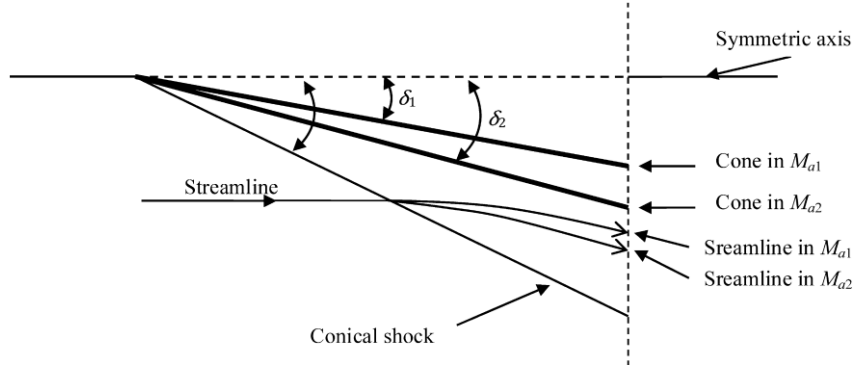
162 subject to the subjective influence of the designer, and there are the problems of high human
163 participation and poor repeatability.

164

165 **3. The variable Mach number waverider**

166 The design method of the variable Mach number waverider is a kind of design method of
167 waveriders with a wide-speed range, which can be combined with different osculating theories in
168 the spanwise direction to obtain the corresponding design method of waveriders with a wide-speed
169 range. The design idea is to design the waverider based on the basic flow field generated by multiple
170 design Mach numbers, so as to achieve the goal of taking into account various flight states for wide-
171 speed flight.

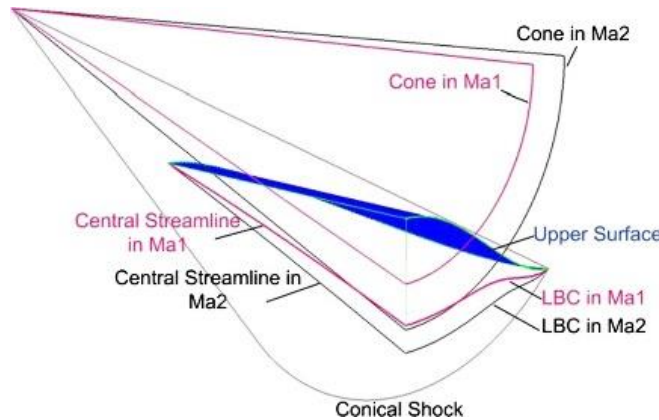
172 In 2017, based on the basic law of conical flow, Zhang et al. [52] first studied the nature of the
173 conical flow field when the Mach number of the free-flow changed, and its effect on the geometry
174 of the generated conical-derived waverider, as shown in Fig. 7. Then, a novel design approach for
175 the wide-speed-range vehicle was proposed on the basis of the design theory of the cone-derived
176 waverider, which is the design method of the conical-derived variable Mach number waverider. The
177 basic design idea is to use a streamline-tracing technique to generate streamlines on the lower
178 surface of the conical-derived variable Mach number waverider in different lateral areas, such that
179 different design Mach numbers are allocated, and then the lower surface of the aircraft is obtained
180 by the lofting method, as shown in Fig. 8.



181

182

(a) The conical flow field



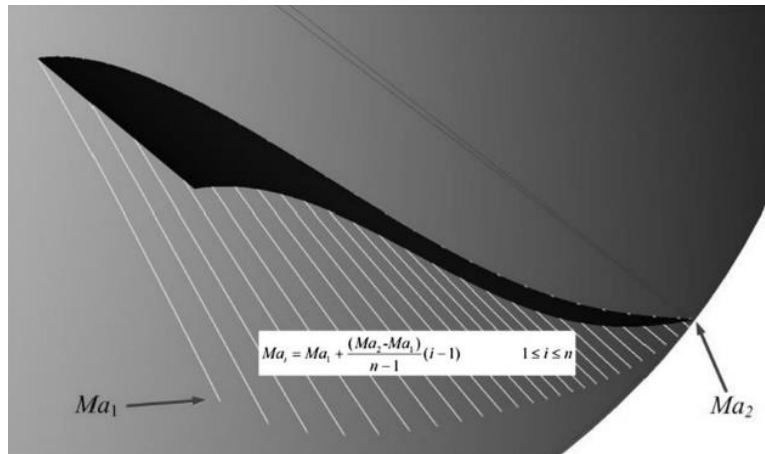
183

184

(b) The configuration of the conical-derived waverider

185

Fig. 7 The effect of the variation of the free stream Mach number [52].



186

187

Fig. 8 The design schematic of the conical-derived variable Mach number waverider [52].

188

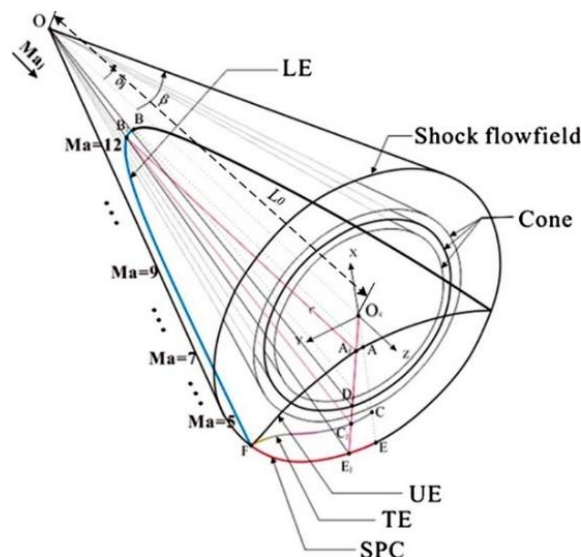
189

190

The numerical simulation results show that the designed conical-derived variable Mach number waverider has better wave-ride properties in the design Mach number range due to the compromised aerodynamic performance compared with the waveriders generated under two

191 ultimate design Mach numbers. In addition, the conical-derived variable Mach number waverider
 192 whose design Mach number decreases from the edge to the vehicle's symmetry plane continuously
 193 has better aerodynamic performance than the one whose design Mach number increases from the
 194 edge to the vehicle's symmetry plane.

195 Subsequently, using similar design ideas, Li et al. [53] also carried out the design of the variable
 196 Mach number waverider. The design steps of the conical-derived variable Mach number waverider
 197 are given in detail, as shown in Fig. 9. The study results indicated that the overall performance of
 198 the variable Mach number waverider is superior in the wide-speed range. The variation of the design
 199 Mach number has a great influence on the aerodynamic performance of the waverider, confirming
 200 the conclusion in Ref. [52]; furthermore, when the thickness of the waverider is kept the same, the
 201 variable Mach number waverider has a stronger shock wave compression ability than the ordinary
 202 waverider.

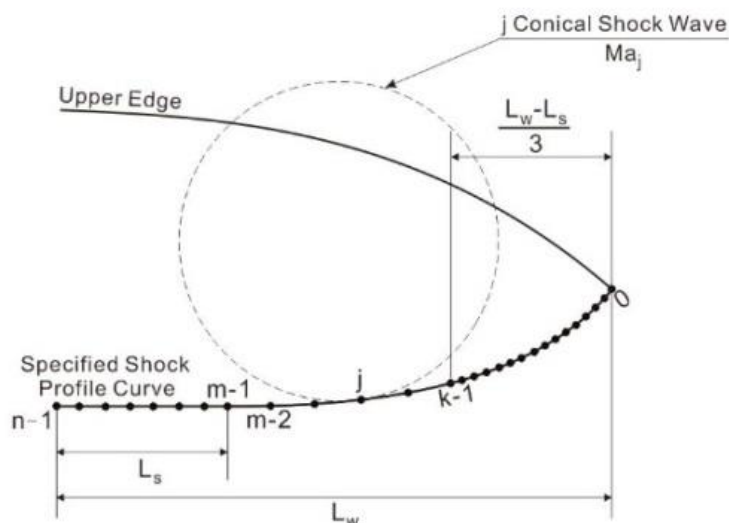


203

204 Fig. 9 Schematic diagram of the variable Mach number waverider generation approach [53].

205 To further expand the application range of the variable Mach number waverider design method,
 206 a novel design method for the wide-speed range waverider, which combines the design method of

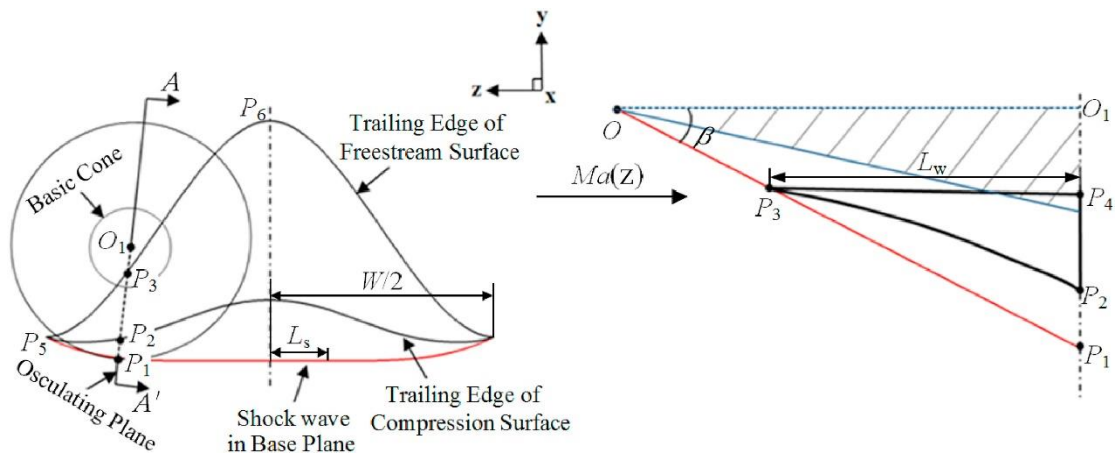
207 the variable Mach number waverider with the osculating cone theory, was proposed by Zhao et al.
 208 [54] in 2018. The design idea is to configure conical flow fields with different free stream Mach
 209 numbers for each osculating plane to obtain the three-dimensional supersonic flow field required
 210 for the design of the osculating cone variable Mach number waverider, as shown in Fig. 10. The
 211 numerical simulation results show that over the whole flight profile, the osculating cone variable
 212 Mach number waverider has a higher lift-to-drag ratio than the conventional osculating cone
 213 waverider with the same volumetric efficiency, which reflects its aerodynamic performance
 214 advantages.



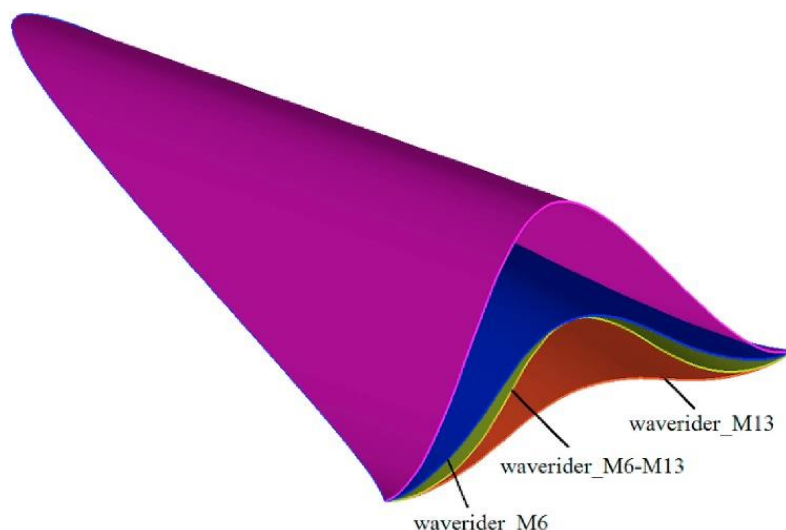
215
 216 Fig. 10 The schematic diagram of the osculating cone variable Mach number waverider [54].

217 Based on the osculating flowfield method for waveriders, a design method for the variable
 218 Mach number waverider was developed by Liu et al. [55] in 2019. The definition of design
 219 parameters for the osculating flowfield waverider used in Liu's waverider design is shown in Fig.
 220 11. Their study results indicated that there is no obvious overflow phenomenon in the design Mach
 221 number range of the variable Mach number osculating flowfield waverider, which indicates that the
 222 aircraft has good waverider properties in the wide- speed range; furthermore, the leading edges of

223 the variable Mach number osculating flowfield waverider are the same as those of the ordinary
 224 osculating cone waverider, but the trailing edges of its compression surface are different, as shown
 225 in Fig. 12. In addition, the variable Mach number osculating flowfield waverider also has a good
 226 balance between its main performance, namely aerodynamic performance and volumetric efficiency,
 227 thus indicating that the aircraft is more suitable for wide-speed range flight.



228
 229 Fig. 11 The design parameters of the osculating flowfield waverider [55].



230
 231 Fig. 12 Configuration comparison of the variable Mach number osculating flowfield waverider
 232 and ordinary osculating cone waverider [55].

233 Generally speaking, the design procedure for a waverider mainly includes the following three
 234 parts: designing and solving the basic flow field, tracing a group of streamlines in the basic flow

235 field, and lofting all the streamlines to generate the upper surface and the compression-stream
236 surface of the vehicle [56]. From this perspective, the design method of the variable Mach number
237 waverider is to improve the wide-speed range characteristics of the waverider by changing the basic
238 flow field. In fact, the original idea of this design method came from Ref. [46]. The first step to
239 generate the "parallel" wide-speed range waverider configuration is to obtain the leading-edges of
240 waveriders for the low and high design Mach numbers. Then, the leading edge of the wide-speed
241 range vehicle is generated by combining the two leading edges in parallel. Secondly, the upper-edge
242 on the back wall for the wide-speed range vehicle is generated according to the corresponding
243 requirements. In the end, lofting all relevant streamlines forms the compression surface. The leading
244 edge and upper-edge on the back wall form the freestream surface, and the upper-edge on the back
245 wall and trailing edge of compression surface form the bottom surface. The trailing edge of the
246 compression surface is obtained by tracking the leading edge to the back wall in the free stream
247 direction. At this point, the design of the "parallel" wide-speed range waverider configuration is
248 complete. Obviously, the second step is not only the key point of the design process, but also the
249 main disadvantage of this design method, that is, there are problems of high human participation
250 and poor repeatability. Therefore, in order to avoid manual splicing, the design method of the
251 variable Mach number waverider is evolved by integrating this parallel design idea into the
252 waverider design method.

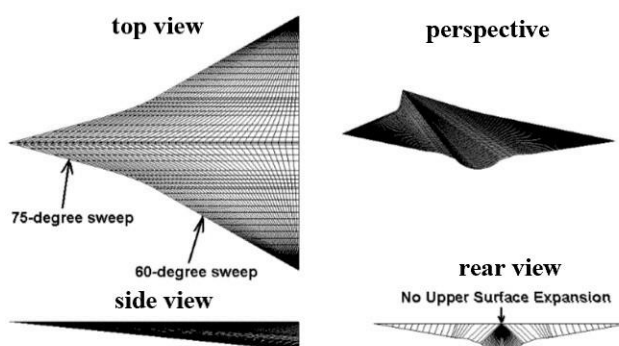
253

254 **4. The vortex lift waverider**

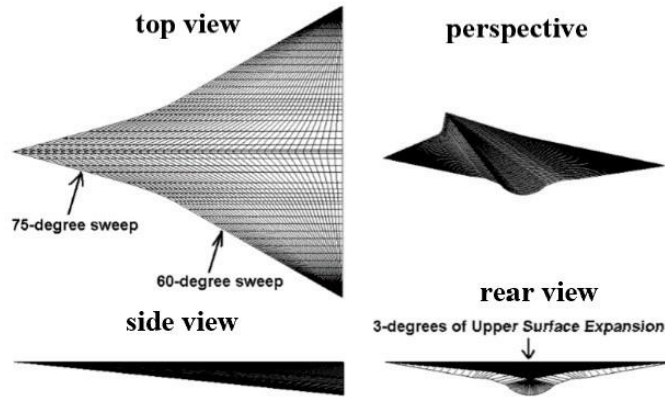
255 It is well known that the non-linear behavior of lift with angle of attack is known as vortex lift,
256 which typically occurs on thin, highly swept, sharp-edged wings used for transonic and supersonic

257 flight [57][58]. In addition, compared with the research efforts on high-speed vortex flows, a
258 primary focus of the low-speed research has been on the use of vortex flows to improve aerodynamic
259 performance [59]. Therefore, the rational use of vortex lift or low-speed vortex flows to design a
260 waverider can be regarded as a method to improve its wide-speed-range characteristics, consistent
261 with the original intention of the vortex lift waverider.

262 In 2005 and 2012, Rodi [25][60] first proposed the concept of the vortex lift waverider and
263 described it as a new type of waveriders which can increase the lift of the vehicle by reducing the
264 pressure on the leeward surface via designing for leading edge vortices. The vortex lift waverider
265 with sweep angle schedules designed to produce strong leading edge vortices can be generated by
266 utilizing the osculating flowfield waverider generation method and defined geometrical
267 relationships to generate specific leading edge sweep angles [61]. In addition, in order to gain the
268 “separation bubble with shock” flow domain that can generate the high lift producing vortices, Rodi
269 [60] proposed two methods. Among them, the first method is to raise the waverider’s angle of attack,
270 and the second method is to include expansion on the leeward side of the waverider. Since the second
271 approach reduces the volume of the vehicle, it is expected to be less desirable. An example using
272 each method is shown in Fig. 13.



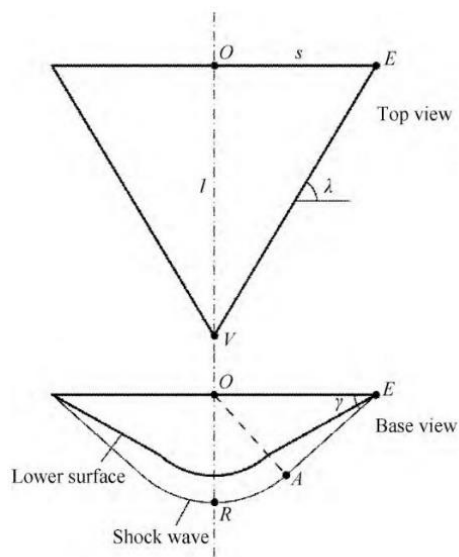
(a) The waverider generated by the first method



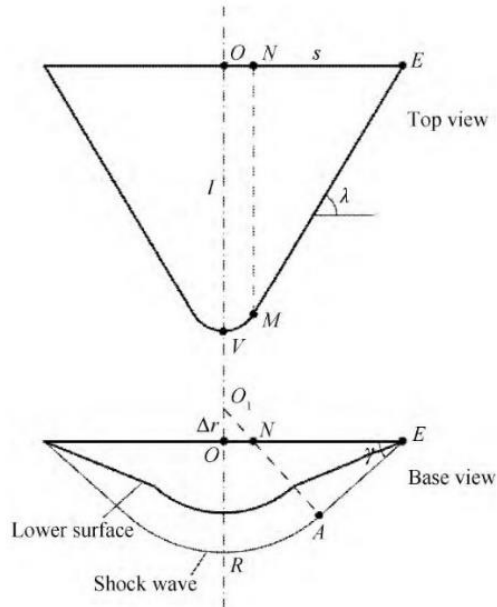
(b) The waverider generated by the second method

273 Fig. 13 The vortex lift waverider with a design Mach number of 6.0 [60].

274 The research in Ref. [60] focuses on the geometric characteristics and on the vortex lift
 275 characteristics of the vortex lift waverider, but the specific method of generating such an aircraft is
 276 not explained. Duan et al. [62] proposed in a detailed method of generating the waverider with
 277 constant angle of sweepback according to the osculating cone theory and the geometric
 278 characteristics of the vortex lift waverider. The design principle of the osculating cone waverider
 279 with constant angle of sweepback is shown in Fig. 14. Its waverider properties and vortex lift
 280 characteristics are verified by computational fluid dynamics (CFD) simulation.



(a) Geometry characteristic of the OCWRCAS I

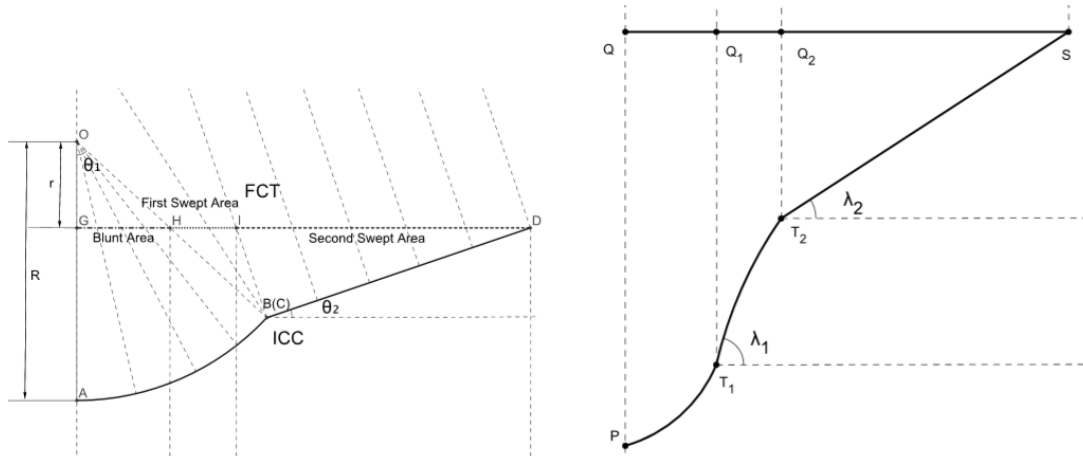


b) Geometry characteristic of the OCWRCAS II

281 Fig. 14 Schematic illustration of generation method of the osculating cone waverider with constant
282 angle of sweepback [62].

283 In 2017, according to the design method for the osculating cone waverider, Liu et al. [63] put
284 forward the concept of the double swept waverider and gave the relationships between design
285 parameters and configuration parameters. Fig. 15 illustrates the design schematic of the double
286 swept waverider. Furthermore, using the non-uniform rational B-spline (NURBS) method to aid in
287 generating the waverider, the design method to create the waverider with controllable configuration
288 parameters (including the blunt head area, the sweep angle and the swept area) was studied. The
289 results showed that the double swept waverider with an appropriate shape can improve its subsonic
290 characteristics, aerodynamic stability and nonlinear vortex lift while maintaining the high
291 hypersonic performance, thus providing a novel way to design the wide-speed range hypersonic
292 vehicles.

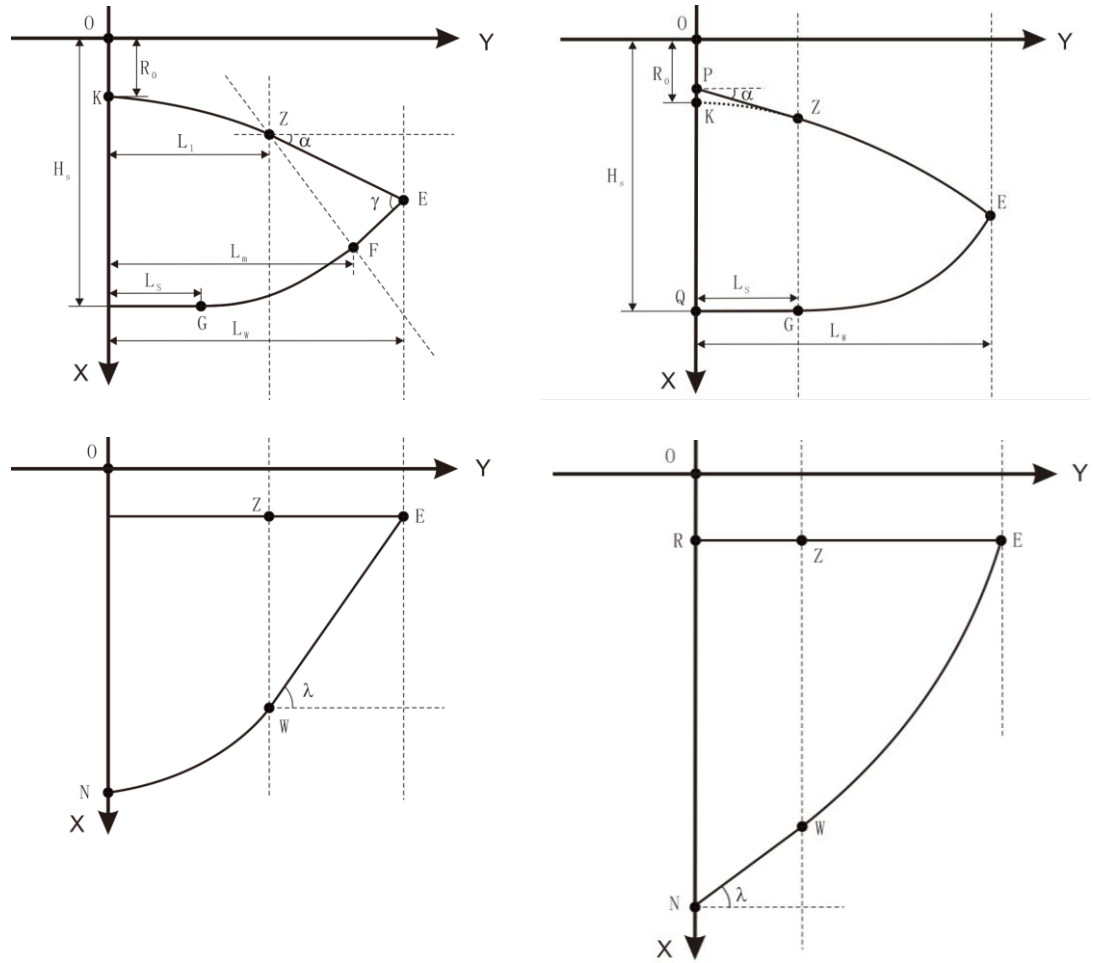
293



294 Fig. 15 Schematic representation of generation method of the double swept waverider [63].

295 In the above two methods of generating the constant swept waverider, the curved portion
 296 constituting the inlet capture curve (ICC) uses a circular arc, and the flow capture tube (FCT) is
 297 designated as a straight line, which severely limits the design space of the vortex lift waverider.
 298 Therefore, according to the geometrical relationship of the osculating cone waverider, Zhao et al.
 299 [64] presented design methods for two kinds of constant swept waveriders with more flexible design
 300 curves (ICC and FCT). They named them the cuspidal waverider and the delta-winged waverider,
 301 respectively. Their principles are illustrated in Fig. 16. Zhao et al. [64] designed a conventional
 302 osculating cone waverider which has the same volumetric efficiency as the delta-winged waverider
 303 and the cuspidal waverider, and they analyzed the performance differences between them. The
 304 comparison results showed that the aerodynamic performance of the cuspidal waverider is better
 305 than that of the general osculating cone waverider under any flight conditions in the high speed
 306 range, while the high speed aerodynamic performance of the delta-winged waverider is worse; the
 307 results also demonstrated that the lift coefficient curve of the cuspidal waverider exhibits a
 308 significant nonlinear increase in the high speed range, while the lift coefficient curves of the delta-
 309 winged waverider and the general osculating cone waverider do not have this property. This

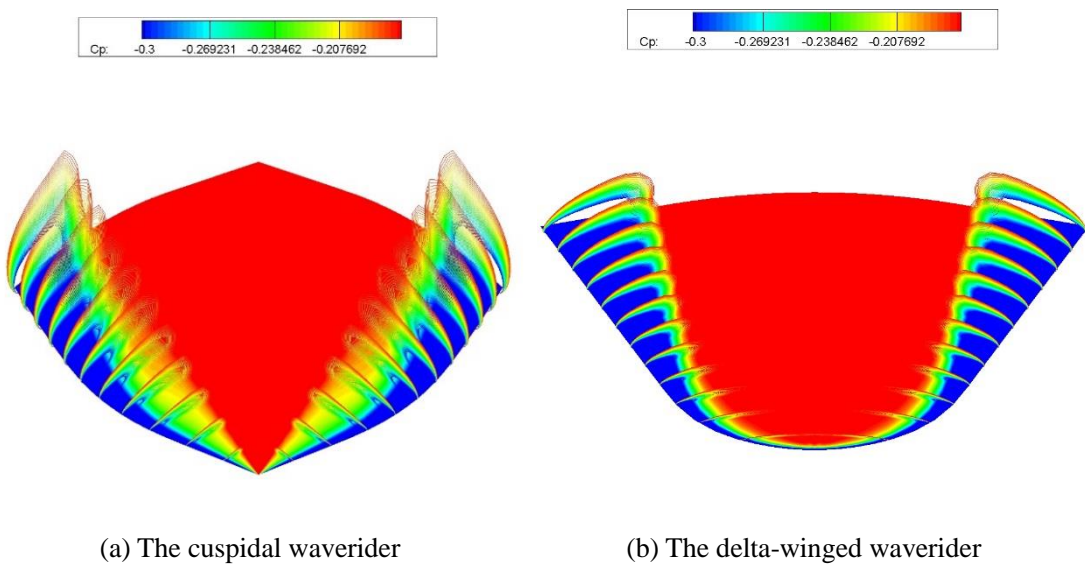
310 indicates that the different positions of the straight line segment in the leading edge of the waverider
 311 has different effects on the high speed aerodynamic performance of the waverider.



(a) Design geometry of the delta-winged waverider (b) Design geometry of the cuspidal waverider

312 Fig. 16 Sketch for the design of the delta-winged waverider and the cuspidal waverider [64].
 313 In addition, in order to further explore the low speed performance advantages of the two types
 314 of vortex lift waverider with a wide-speed range designed in Ref. [64], Zhao et al. [65] used the
 315 CFD approach to analyze the low speed viscous flow fields, the vortex lift characteristics, and the
 316 low speed viscous aerodynamic performances of the cuspidal waverider, delta-winged waverider
 317 and general osculating cone waverider. The analysis results indicated that the low speed lift-to-drag
 318 ratio of the cuspidal waverider is higher than that of the general osculating cone waverider with the

319 same volumetric efficiency, while the low speed lift-to-drag ratio of the delta-winged waverider is
 320 lower. Moreover, the cuspidal waverider better balances the low-speed takeoff performance and the
 321 high speed cruise performance, further enlarging its own flight speed range, while the low-speed
 322 takeoff performance of the delta-winged waverider is poor, which is mainly caused by the
 323 differences in the low speed vortex structure of the three types of aircraft. Fig. 17 shows the low
 324 speed vortex structure of the cuspidal waverider and the delta-winged waverider under the flight
 325 condition.



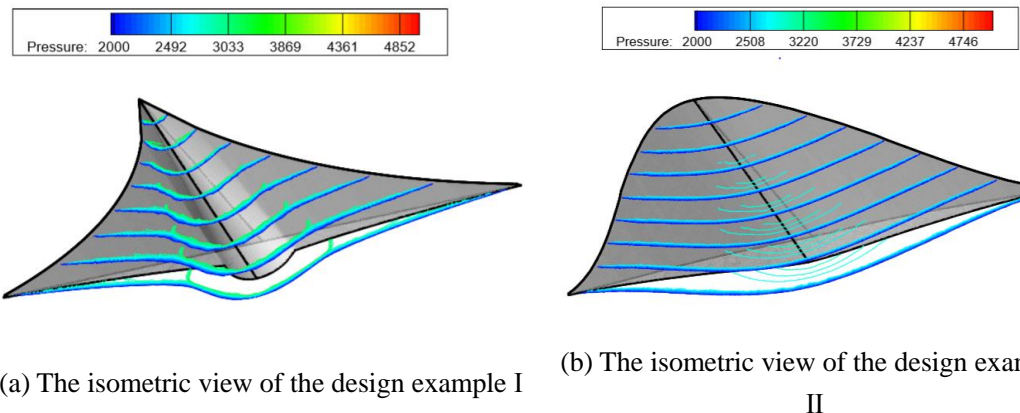
326 Fig. 17 The low speed vortex structure of the cuspidal waverider and the delta-winged waverider
 327 [65].

328 On the other hand, considering that the shape of the aircraft, especially the planar shape, has a
 329 great influence on the aerodynamic and maneuvering characteristics of the aircraft, Liu et al. [66][67]
 330 developed the concept of the double swept waverider proposed in Ref. [63] and put forward the
 331 concept of the planform-customized waverider. Its design is based on a set of differential equations
 332 derived from the global geometric relationships among the inlet capture curve (ICC), flow capture
 333 curve (FCC) and planar shape curve (PSC) in the osculating-cone waverider design. This waverider

334 design method can be used in the design of the wide-speed range waverider. The main idea is to
335 introduce the vortex effect by customizing the planform for the waverider, thereby employing the
336 vortex effect to improve the low speed aerodynamic performance and the shock effect to improve
337 the super/hypersonic aerodynamic performance, respectively. The double swept waverider can be
338 used to verify the correctness of this design concept. They then performed a comparison study of
339 the double swept waverider and flat plate model using computational fluid dynamics (CFD)
340 simulation. The study results showed that the aerodynamic performances of the waverider with
341 reasonable planform is favorable under both subsonic and hypersonic conditions, remedying some
342 deficiencies of the traditional waverider.

343 On this basis, Wang et al. [68] studied the design method for the waverider with a controllable
344 planar shape as a new waverider design method, i.e., the design of the waverider is carried out by
345 solving the differential equation set in the planform-customized waverider design method. Their
346 design method introduced the planar shape as a design-driving parameter instead of being
347 determined by the FCC and the ICC to improve the waverider design flexibility. In order to improve
348 the low-speed lift-to-drag ratio of the waverider to satisfy take-off and landing requirements, larger
349 aspect ratio and smaller sweep angle are beneficial to improve the low-speed performance of aircraft.
350 Therefore, two kinds of waverider with the low-speed-friendly planar shape (one with a decrease of
351 leading edge sweep angle and an “ \int ” -like one) were designed by using the design method of the
352 waverider with a controllable planar shape. Fig. 18 illustrates the two waverider configurations with
353 the low-speed-friendly planar shape. The results showed that customizing the planar shape does not
354 destroy the favorable characteristics of the waverider, i.e., the waverider with a controllable planar
355 shape still has a superior high lift-to-drag ratio in the hypersonic speed range; in addition, the low

356 speed aerodynamic performance is significantly improved as compared to the one without using a
 357 low-speed-friendly planar shape, and the performance improvement is achieved at lower cost,
 358 because the planar shapes are specified by an engineering point of view instead of complex
 359 optimization related to conventional waverider designs.



360 Fig. 18 The configuration of the waverider with the low-speed-friendly planar shape [68].
 361

362 5. The dual/multistage waverider

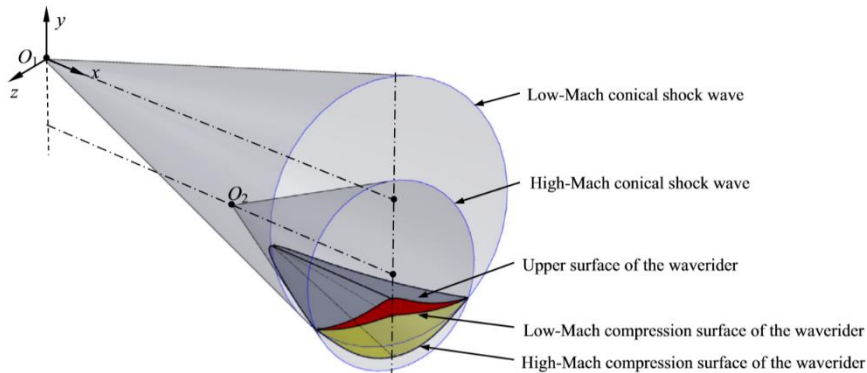
363 Hypersonic vehicles can be divided into unpowered gliding and powered cruising vehicles
 364 according to whether there is an engine that provides thrust in flight [69]. By combining the
 365 advantages of the gliding and cruising flights, Xu et al. [69] proposed a new type of flight trajectory
 366 scheme and applied it to the hypersonic gliding-cruising vehicle. The new flight scheme is that the
 367 vehicle itself, according to the above concept, is equipped with a ramjet engine with fixed thrust
 368 and multiple start functions, and glides and re-enters from outer space at hypersonic speeds; when
 369 it arrives within a certain distance from the target or decelerates to a velocity below a specific
 370 velocity, the activated ramjet engine propels the vehicle to cruise at hypersonic speeds.

371 The waverider design process reveals that there is a single corresponding relationship between
 372 the shape of the waverider and the design input parameters, that is, a set of input parameters

373 corresponds to the unique shape of the waverider. In the flight trajectory scheme of the hypersonic
374 gliding-cruising vehicle, there are two different main flight phases, namely, the high Mach number
375 gliding flight phase and the low Mach number cruise flight phase. Therefore, in this new flight
376 scheme, the conventional waverider cannot take advantage of its high lift-to-drag ratio. In order to
377 find the most suitable aerodynamic configuration for the gliding-cruising ballistic waverider, the
378 design concept of the dual/multistage waverider was proposed. Its objective was to design the inlet
379 shroud in the gliding stage into the waverider's compression surface.

380 In 2014, Liu et al. [70] proposed a new waverider design concept, namely a dual waverider.
381 The term 'dual waverider' here refers to a gliding and cruising waverider. Its design idea is to regard
382 the gliding Mach number of the dual waverider as the design Mach number. The inlet shroud is
383 designed as to serve the compression surface of the waverider by using the design method of the
384 cone-derived waverider to ensure that the dual waverider can ride on the shock wave during the
385 gliding phase, and therefore can maintain the waverider characteristics at the design gliding Mach
386 number. On the other hand, using the cruising Mach number of the dual waverider as the design
387 Mach number, the forebody is also designed as the waverider's compression surface by applying
388 the cone-derived waverider's design method to ensure that the dual waverider can still ride on the
389 shock wave after the inlet shroud is cast away. The schematic diagram of the dual waverider design
390 method based on the design theory of the cone-derived waverider is shown in Fig. 19. Liu et al. [70]
391 then verified this waverider design method via numerical simulation, and subsequently compared
392 and analyzed both the dual waverider and the conventional waverider. The study showed that the
393 lift coefficient, drag coefficient and lift-to-drag ratio of the gliding waverider are larger than those
394 of the conventional waverider within the -2 °to 6 °angle of attack range. Therefore, this methodology

395 is very helpful for the design of the hypersonic glide-cruise vehicle.



396

397 Fig. 19 The schematic diagram of the dual waverider design method based on the design theory of
398 the cone-derived waverider [70].

399 However, the dual waverider design method proposed by Liu et al. [70] has the following
400 shortcomings: First, the design method of the cone-derived waverider requires that the shock profile
401 curve (SPC) must be an arc, which cannot be easily adjusted to actual needs, and thus complicates
402 to the integrated design of the waverider and the inlet; second, the geometric constraints of this
403 method are very complicated, resulting in the difficulty of designing a suitable dual waverider for
404 the actual mission requirements. In order to solve these problems, Wang [71] adopted the osculating
405 cone theory to design and study the dual waverider, and proposed the dual waverider design methods
406 with constant shock wave angles and variable shock wave angles. The core of these two design
407 methods is to use the osculating cone theory to ensure that the gliding and cruising waverider share
408 a common leading edge.

409 The design idea of the osculating cone dual waverider with constant shock wave angles is as
410 follows: firstly, the basic curves and design parameters are given, wherein the basic curves include
411 the shock profile curve of the cruising waverider and the trailing edge curve of free-stream surface,
412 and the design parameters include the design Mach numbers and shock wave angles of the gliding

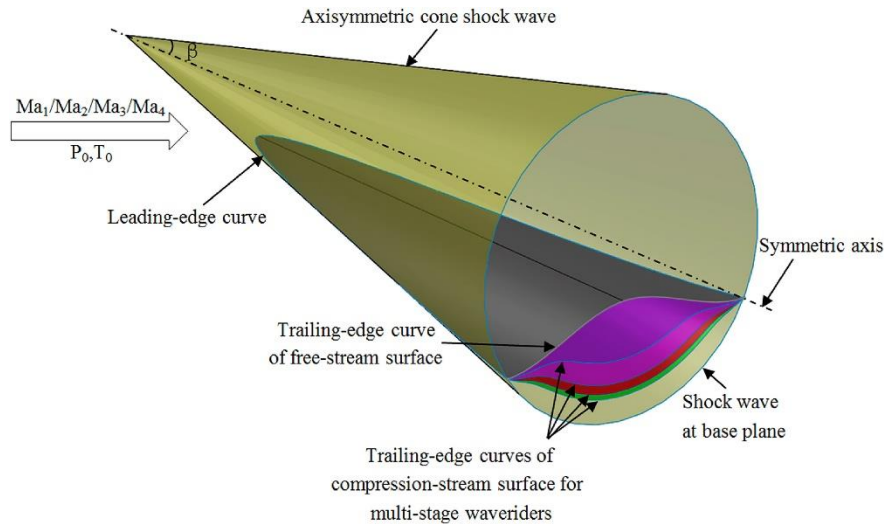
413 and cruising waverider; then, the cruising waverider is designed by the osculating cone theory, and
414 the leading edge of the cruising waverider is obtained; finally, the compression-stream surface of
415 the gliding waverider is designed through the obtained leading edge to ensure that the cruising
416 waverider and the gliding waverider share the same leading edge. The detailed design steps can be
417 found in Ref. [72]. The correctness of this design method is verified by numerical simulation.
418 However, there is flow spillage around the leading edges of the gliding waverider designed by this
419 method. The root cause of this problem is that the design method of the osculating cone dual
420 waverider with constant shock wave angles adopts the following assumptions: the osculating planes
421 of the cruising waverider and the gliding waverider at any point on the trailing edge curve of free-
422 stream surface of the dual waverider are in the same plane, and the osculating cone axis of the
423 gliding waverider in the osculating plane is the same as that of the cruising waverider.

424 In order to remedy the above-mentioned flow spillage, Wang [71] proposed the design method
425 of the osculating cone dual waverider with variable shock wave angles. The design idea is as follows:
426 firstly, the basic curves and design parameters are given, and the cruising waverider is designed by
427 the osculating cone theory, and the leading edge of the cruising waverider is obtained; then,
428 according to the leading edge of the cruising waverider and the shock profile curve of the gliding
429 waverider, the respective shock wave angle are determined in each of the osculating planes, thereby
430 obtaining the basic flow field of the gliding waverider by the osculating cone theory; finally, the
431 streamline tracking method is used to generate the compression-stream surface of the gliding
432 waverider in the basic flow field of the gliding waverider. The detailed design steps can be found in
433 Ref. [73]. The correctness of this design method is verified by the CFD method. From the numerical
434 simulation results, it can be seen that there is no flow spillage around the leading edges of the gliding

435 waverider designed by this method, which indicates that the design method has achieved the original
436 design objective.

437 In 2017, Liu et al. [74] developed the design concept of the dual waverider, and put forward
438 the design method of the multistage waverider. However, the design idea of the multistage waverider
439 is different from that of the dual waverider, and the core of its design is to generate several
440 compression-stream surfaces of the multistage waverider in a plurality of conical flow fields with
441 the same shock angle and different Mach numbers. It can be seen that the multistage waverider
442 design method proposed by Liu et al. [74] can also be regarded as a design method for the variable
443 Mach number waverider. This multistage waverider can be used in two transfiguration flight
444 strategies: one is the application of smart materials and structures in the manufacture of the
445 multistage waverider. By using smart materials, the multistage waverider can appropriately change
446 its configuration according to flight mission requirements, that is, to shape the compression-stream
447 surface, in such a way that the waverider characteristics can be maintained at each flight Mach
448 number. Another transfiguration flight strategy is to use the compression-stream surface at different
449 stages as cowlings when the multistage waverider is used as a gliding vehicle, to ensure that the
450 multistage waverider can always use the compression-stream surface to maintain the waverider
451 characteristics at different flight Mach numbers. It should be noted that the implementation of the
452 former or other transfiguration flight strategies changes the configuration. Therefore, this multistage
453 waverider can be regarded as a morphing waverider. The supersonic axisymmetric conical flow field
454 used in the design of the multistage waverider is shown in Fig. 20. The specific steps of the
455 multistage waverider design method can be found in Ref. [75]. Numerical studies of this kind of
456 waverider and of the traditional single-stage waverider were conducted. The results indicated that

457 the multistage waverider design method can effectively solve the problem of aerodynamic
 458 performance deterioration of the waverider in the off-design state, and ensure that the aircraft always
 459 maintains the optimal flight state.



460

461 Fig. 20 Basic design principle of the multistage waverider [75].

462 In the above schemes, the compression-stream surface of the dual/multistage waverider are
 463 designed for several discrete design Mach numbers, and the waverider characteristics are realized
 464 by using the corresponding compression-stream surface at different flight Mach numbers. This type
 465 of design method can obviously improve the aerodynamic performance of the waverider under the
 466 corresponding design Mach numbers, but it is only a compromise solution, that is, the waverider
 467 characteristics cannot be effectively guaranteed when flying between different design Mach
 468 numbers.

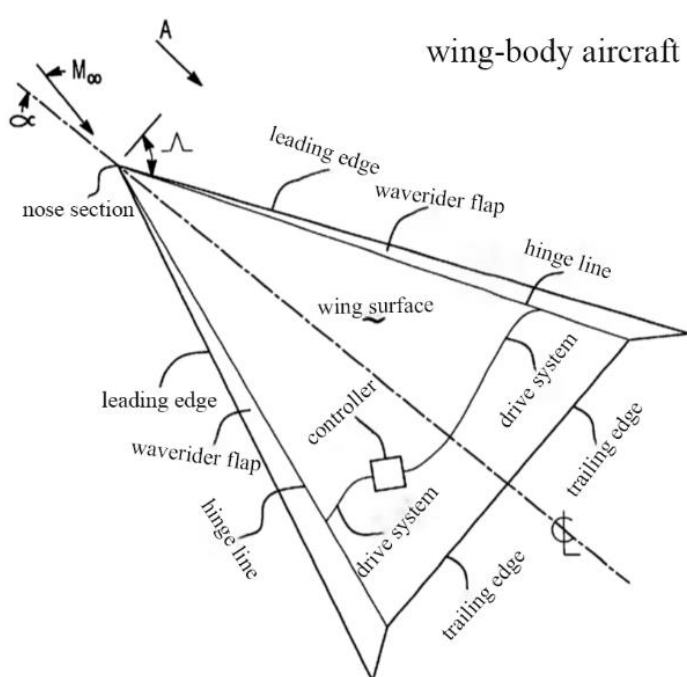
469

470 6. The morphing waverider

471 The term “morphing aircraft” refers to various air vehicles and vehicle components that meet
 472 the requirements of planned and unplanned multipoint missions [76]. It is considered to be a
 473 promising enabling technology for the future, next-generation aircraft [77]. Compared with the

474 traditional aircraft, the morphing aircraft can operate under different flight conditions, which
475 expands its flight envelope [78][79]. They can bridge the design contradiction between high-speed
476 and low-speed flight. Therefore, the use of morphing technologies to enable the waverider to operate
477 over a wide-speed range is quite attractive.

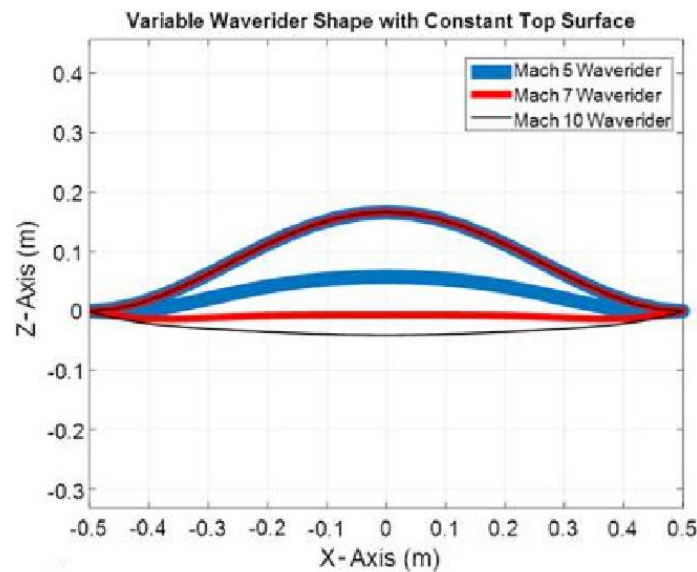
478 In 2003, Bowcutt [80] designed a wing-body aircraft that includes a pair of leading edges, a
479 pair of trailing edges and a pair of waverider flaps, as shown in Fig. 21. Among them, the special
480 configuration of waverider flaps is intended to expand the range of flight Mach numbers and angles
481 of attack while keeping the wing bow shock wave always attached to leading edges. In other words,
482 the purpose of the waverider flaps being articulated is to define an almost infinite number of optimal
483 shapes for the entire range of Mach number and angle of attack required for the wing-body aircraft
484 to operate. In the detailed description of the preferred embodiments, he also pointed out that port
485 and starboard waverider flaps can be actuated independently for greater lateral/directional dynamic
486 stability and control.



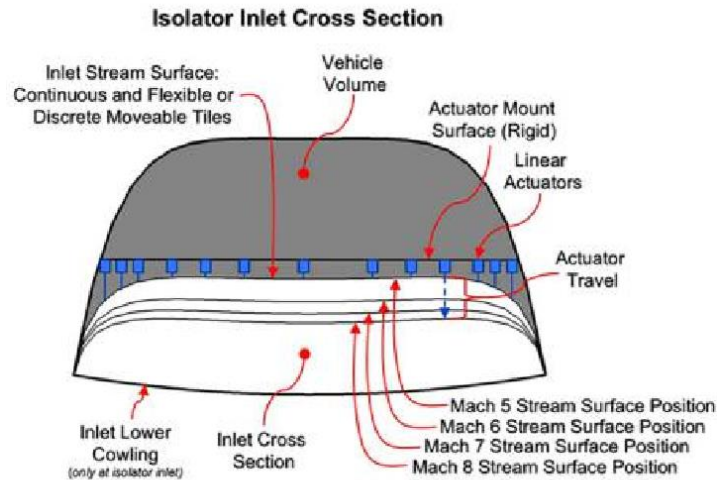
487

488 Fig. 21 The delta wing with waverider flaps as leading edge [80].

489 In 2016, Maxwell [81] proposed a morphing waverider concept that uses a morphing bottom
490 surface to provide on-design waverider aerodynamic performance across a wide Mach number
491 range. The design idea is based on the fact that the total area of the waverider's lower surface stays
492 approximately constant in the hypersonic regime even though the stream surface curvature may vary
493 drastically with the Mach number. On this foundation, the Naval Research Laboratory developed a
494 family of morphing waveriders with a constant leading edge and a constant top surface, as well as
495 a morphing bottom surface [82][83]. Fig. 22 illustrates the general concept of the shape morphing
496 waverider.



(a) waverider projectile



(b) waverider scramjet inlet

497

Fig. 22 The variable waverider shapes [82][83].

498

Next, Phoenix et al. [82][83] investigated the feasibility of the morphing waverider concept

499

and studied the performance advantages of the morphing hypersonic waverider. They used a Finite

500

Element Model (FEM) to model the morphing surface and calculated the resulting morphing

501

accuracies for various control configurations. They designed a Mach 10 waverider to enable shock

502

attachment from Mach 10 to 5 and identified a control set that can accurately control the morphed

503

surface. They analyzed the optimal control points set (actuator locations) and performed a sensitivity

504

analysis using the Q-DEIM-algorithm sensitivity analysis. The study showed that the performance

505

of the ideal morphing waverider is significantly improved and a two-control-point or six-control-

506

point system provides 90% and 97% of the ideal control system performance improvements.

507

It should be noted that at this stage of the above analysis, only the bottom surface of the back

508

cross-section is evaluated, and the full 3D surface is not addressed. Therefore, in order to further

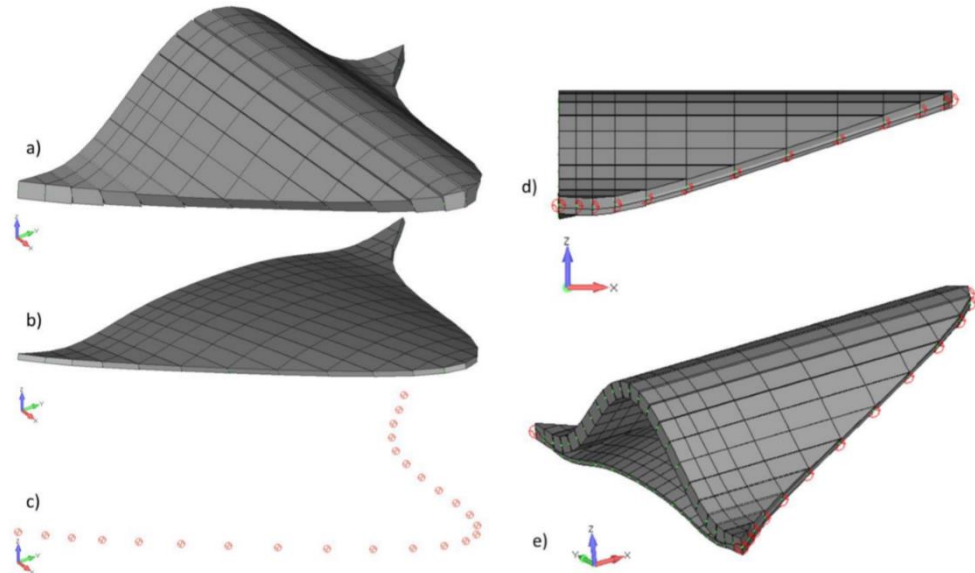
509

determine the validity of the morphing waverider concept, Phoenix et al. [84] also chose a 3D

510

waverider model with realistic system stiffness and geometric constraints to evaluate the locations

511 and number of actuators required to deliver the needed morphing accuracy. The 3D waverider model
 512 that is composed of plate elements with two different thickness and spring elements connections is
 513 shown in Fig. 23. The study indicated that for the six inches wide morphing hypersonic waverider
 514 that was operated from Mach 5 down to Mach 3.5, the surface errors for the cases with 5 and 14
 515 control points were reduced by 87% and 95% respectively. In addition to the research on the
 516 morphable waverider design theory, they also carried out research on the use of a morphable
 517 waverider for entry vehicles and scramjet engine intake manifolds [8][85][86][87][88].



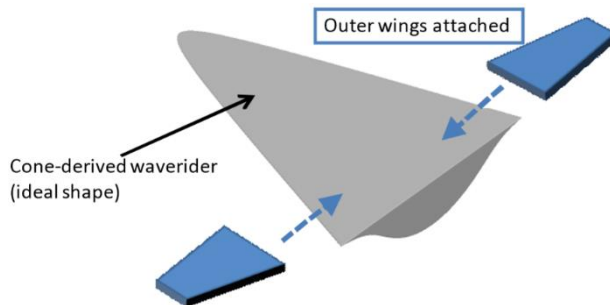
518
 519 Fig. 23 The 3D waverider model with a) Top Surface, b) Bottom Surface, c) Spring Element
 520 Connection between Top and Bottom Surface, d) Combined Model Side view, and e) Isometric
 521 Combined Model View [84].
 522

523 7. Other wide-speed-range waverider designs

524 In addition to the above-mentioned design schemes of waveriders with a wide-speed range,
 525 there are the following additional design schemes.

526 In 2011, Takama [89] proposed to improve the ideal waverider's low-speed aerodynamic

527 characteristics. Its configuration is shown in Fig. 24. He applied numerical simulation to obtain the
528 subsonic and hypersonic aerodynamic performance of this configuration. The results showed that
529 the addition of outer wings can increase the ideal waverider's lift-to-drag ratio in the subsonic regime,
530 while having little effect on its hypersonic performance. Thus, this design concept can be promising
531 for the design of wide-speed-range hypersonic waveriders.



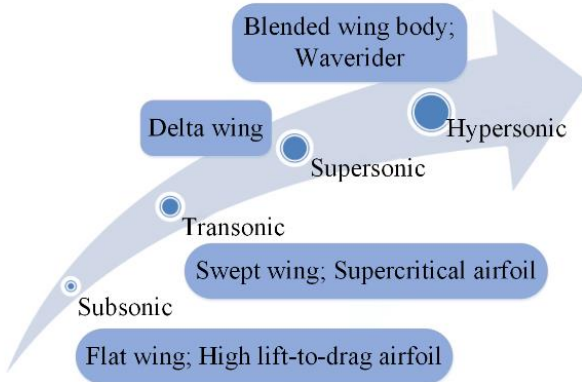
532

533 Fig. 24 The practical waverider attached to outer wings [89].

534

535 8. Discussion

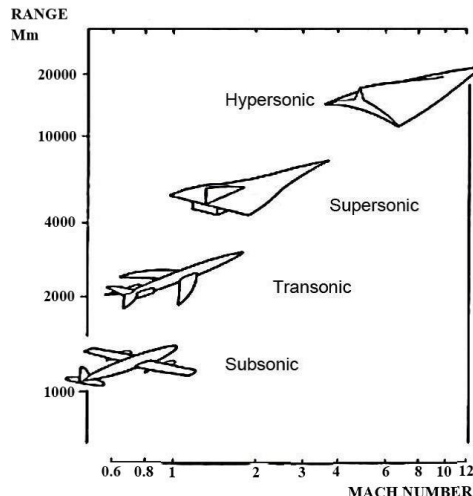
536 The aerodynamic characteristics of an aircraft are closely related to its flight speed range. As
537 shown in Figs.25 and 26, the optimized aerodynamic configurations are quite different in different
538 speed ranges. Therefore, combining the configuration characteristics of the aircraft in different flight
539 speed ranges can be used as a development idea to find the optimal wide speed range waverider
540 configuration.



541

542

Fig. 25 Optimal aerodynamic configuration at different speed ranges.



543

544

Fig. 26 The aircraft pedigree [1].

545 To this end, a good understanding of the non-linear behavior of the vortex generated lift as
 546 discussed in Ref. [25] and Refs.[55-63], is very important. As discussed in Ref. [90], the
 547 aerodynamic performance of the waverider is closely related to the aerodynamic state of its leading
 548 edge, that is, to the average aspect ratio of the waverider. When the leading edge of the waverider
 549 is subsonic, the flow field exhibits typical characteristics of a subsonic flow field, and its lift is
 550 mainly derived from leading edge vortices near the leading edge of the upper surface. On the other
 551 hand, when the leading edge is supersonic, the compression effect of the shock near the leading

552 edge becomes the main source of the lift of the waverider. Therefore, another development idea of
553 the wide-speed range waverider is to analyze and study the characteristics of vortex flow around the
554 waverider, and then design a waverider which can effectively employ the vortex effect to improve
555 the subsonic performance and the shock effect to improve the super/hypersonic performance,
556 respectively. For example, the study in Ref. [66] is a design that combines vortex lift and
557 compression lift to improve the aerodynamic performance of the waverider over a wide-speed range.

558

559 **9. Conclusions**

560 In this survey, the research progress on the design methodology of wide-speed-range
561 hypersonic vehicles based on the design method of waveriders has been summarized, and five
562 typical design schemes have been mentioned, namely the “combined” wide-speed range waverider,
563 the variable Mach number waverider, the vortex lift waverider, the dual/multistage waverider, and
564 the morphing waverider. Their design ideas and characteristics have been introduced and analyzed.
565 For the further development of the wide-speed range waverider, the following conclusions are
566 important:

- 567 ● Considering that the flight characteristics at different flight speeds are quite different, it will
568 be important to effectively combine the aerodynamic characteristics of the aircraft in
569 different flight speed ranges.
- 570 ● The method of applying the vortex lift concept to the design of the waverider still requires
571 further study. The generation, development and influencing factors of the vortex effect need
572 to be more deeply analyzed.
- 573 ● The morphing technologies and the recent advances in smart materials research, actuation

574 technology, constitutive laws and modeling, optimization and control, and failure prediction,
575 will become increasingly important for the design of the wide-speed-range hypersonic
576 vehicle.

577

578 **Conflict of interest statement**

579 The authors declare there is no conflict of interest regarding the publication of this paper.

580

581 **Acknowledgements**

582 The authors would like to express their thanks for the support from the National Key R&D
583 Program of China (No.2019YFA0405300) and the National Natural Science Foundation of China
584 (No.11972368). Also, the authors thank the reviewers for their constructive recommendations and
585 Prof. Platzer for his assistance in editing the paper.

586

587 **References:**

- 588 [1]. Küchemann D. The aerodynamic design of aircraft. **Pergamon Press**, 1978
- 589 [2]. Szirocak D, Smith H. A review of design issues specific to hypersonic flight vehicles.
590 **Progress in Aerospace Sciences**, 2016, 84: 1-28
- 591 [3]. Lunan D, A M, Ed D. Waverider, a revised chronology. **20th AIAA International Space Planes
592 and Hypersonic Systems and Technologies Conference**, AIAA Paper 2015-3529, 2015
- 593 [4]. Knittel J. Aero-assisted spacecraft missions using hypersonic waverider aeroshells. Doctoral
594 Dissertation, University of Maryland, College Park, 2015
- 595 [5]. Ferguson F, Corbett T, Akwaboa S, et al. The development of waveriders from an axisymmetric

- 596 flowfield. **45th AIAA Aerospace Science Meeting and Exhibit**, AIAA Paper 2007-847, 2007
- 597 [6]. Rodi P E. Integration of optimized leading edge geometries onto waverider configurations.
- 598 **53rd AIAA Aerospace Sciences Meeting**, AIAA Paper 2015-1700, 2015
- 599 [7]. Maxwell J R. Efficient design of hypersonic waveriders with CFD verification and off-design
- 600 performance analysis. **53th AIAA/SAE/ASEE Joint Propulsion Conference**, AIAA Paper
- 601 2017-4879, 2017
- 602 [8]. Maxwell J R, Phoenix A A. Morphable hypersonic waverider and trajectory optimized for
- 603 atmospheric entry. **AIAA SPACE and Astronautics Forum and Exposition**, AIAA Paper
- 604 2017-5357, 2017
- 605 [9]. Huang G P, Zuo F Y, Qiao W Y. Design method of internal waverider inlet under non-uniform
- 606 upstream for inlet/forebody integration. **Aerospace Science and Technology**, 2018, 74: 160-
- 607 172
- 608 [10]. Rodi P E. High lift-to-drag ratio waveriders for missions in the Martian atmosphere. **30th AIAA**
- 609 **Applied Aerodynamics Conference**, AIAA Paper 2012-3221, 2012
- 610 [11]. Stevens D R. Practical considerations in waverider applications. **AIAA Aircraft Design**
- 611 **Systems Meeting**, AIAA Paper 92-4247, 1992
- 612 [12]. Lobbia M A. Multidisciplinary design optimization of waverider-derived crew reentry vehicles.
- 613 **Journal of Spacecraft and Rockets**, 2017, 54(1): 233-245
- 614 [13]. Bowcutt K G, Anderson J D, Capriotti D. Viscous optimized hypersonic waveriders. **25th**
- 615 **AIAA Aerospace Sciences Meeting**, AIAA Paper 87-0272, 1987
- 616 [14]. Liu W, Zhang C A, Wang F M. Modification of hypersonic waveriders by vorticity-based
- 617 boundary layer displacement thickness determination method. **Aerospace Science and**

- 618 **Technology**, 2018, 75: 200-214
- 619 [15].Anderson J D, Lewis M J, Kothari A P, et al. Hypersonic waveriders for planetary atmospheres.
- 620 **Journal of Spacecraft and Rockets**, 1991, 28(4): 401-410
- 621 [16].Rasmussen M L. Waverider configurations derived from inclined circular and elliptic cones.
- 622 **Journal of Spacecraft and Rockets**, 1980, 17(6): 537-545
- 623 [17].He X Z, Le J L, Wu Y C. Design of a curved cone derived waverider forebody. **16th AIAA/DLR/DGLR International Space Planes and Hypersonic Systems and Technologies Conference**, AIAA Paper 2009-7423, 2009
- 626 [18].You Y C, Zhu C X, Guo J L. Dual waverider concept for the integration of hypersonic inward-turning inlet and airframe forebody. **16th AIAA/DLR/DGLR International Space Planes and Hypersonic Systems and Technologies Conference**, AIAA Paper 2009-7421, 2009
- 629 [19].He X Z, Zhou Z, Qin S, et al. Design and experimental study of a practical Osculating Inward Cone Waverider Inlet. **Chinese Journal of Aeronautics**, 2016, 29(6): 1582-1590
- 631 [20].Ding F, Liu J, Shen C B, et al. Novel approach for design of a waverider vehicle generated from axisymmetric supersonic flows past a pointed von Karman ogive. **Aerospace Science and Technology**, 2015, 42: 297-308
- 634 [21].Kontogiannis K, Søbester A, Taylor N. Efficient parameterization of waverider geometries. **Journal of Aircraft**, 2017, 54(3): 890-901
- 636 [22].Chauffour M L, Lewis M J. Corrected waverider design for inlet applications. **40th AIAA/ASME/SAE/ASEE Joint Propulsion Conference and Exhibit**, AIAA Paper 2004-3405, 2004
- 639 [23].Kontogiannis K, Søbester A, Taylor N. On the conceptual design of waverider forebody

- 640 geometries. **53rd AIAA Aerospace Sciences Meeting**, AIAA Paper 2015-1009, 2015
- 641 [24]. Sobieczky H, Dougherty F C, Jones K. Hypersonic waverider design from given shock waves.
- 642 **First International Hypersonic Waverider Symposium**, 1990
- 643 [25]. Rodi P E. The osculating flowfield method of waverider geometry generation. **AIAA-2005-0511**, Reno: AIAA, 2005
- 644 [26]. Rodi P E, Genovesi D J. Engineering-based performance comparisons between osculating cone and osculating flowfield waveriders. **37th AIAA Fluid Dynamics Conference and Exhibit**, AIAA Paper 2007-4344, 2007
- 645 [27]. Rodi P E. On using upper surface shaping to improve waverider performance. **2018 AIAA Aerospace Sciences Meeting**, AIAA Paper 2018-0554, 2018
- 646 [28]. Rodi P E. Waverider vehicle optimization with volumetric constraints for wave drag minimization. **2018 AIAA Aerospace Sciences Meeting**, AIAA Paper 2018-1048, 2018
- 647 [29]. Clegg J, Rodi P E, Meade A. Validation of a crossflow velocity model between waverider flowfield planes. **2019 AIAA Aviation Forum**, AIAA Paper 2019-2813, 2019
- 648 [30]. Rodi P E. An examination of crossflow between waverider flowfield planes. **22nd AIAA International Space Planes and Hypersonics Systems and Technologies Conference**, AIAA Paper 2018-5196, 2018
- 649 [31]. Rodi P E. Expanding the osculating flowfield waverider method beyond power law body induced flowfields. **2018 Applied Aerodynamics Conference**, AIAA Paper 2018-3817, 2018
- 650 [32]. Cui K, Hu S C, Li G L, et al. Conceptual design and aerodynamic evaluation of hypersonic airplane with double flanking air inlets. **Sci China Tech Sci**, 2013, 56(8): 1980-1988
- 651 [33]. Rodi P E. Waverider vehicle optimization with volumetric constraint for sonic boom. **2018**

- 662 **AIAA Aerospace Sciences Meeting**, AIAA Paper 2018-0551, 2018
- 663 [34]. Wang X D, Wang J F, Lyu Z J. A new integration method based on the coupling of multistage
664 osculating cones waverider and Busemann inlet for hypersonic airbreathing vehicles. **Acta
665 Astronaut**, 2016, 126: 424-438
- 666 [35]. Javaid K H, Serghides V C. Airframe-propulsion integration methodology for waverider-
667 derived hypersonic cruise aircraft design concepts. **Journal of Spacecraft and Rockets**, 2005,
668 42(4): 663-671
- 669 [36]. Takashima N, Lewis M J. Waverider configurations based on non-axisymmetric flow fields for
670 engine-airframe integration. **32nd Aerospace Sciences Meeting and Exhibit**, AIAA Paper
671 1994-0380, 1994
- 672 [37]. Takashima N, Lewis M J. Engine-airframe integration on osculating cone waverider-based
673 vehicle designs. **32nd Joint Propulsion Conference and Exhibit**, AIAA Paper 1996-2551,
674 1996
- 675 [38]. O'Brien T F, Lewis M J. RBCC engine-airframe integration on an osculating cone waverider
676 vehicle. **36th AIAA/ASME/SAE/ASEE Joint Propulsion Conference and Exhibit**, AIAA
677 Paper 2000-3823, 2000
- 678 [39]. O'Neill M K, Lewis M J. Design tradeoffs on scramjet engine integrated hypersonic waverider
679 vehicles. **Journal of Aircraft**, 1993, 30(6): 943-952
- 680 [40]. Tarpley C, Lewis M J. Optimization of an engine-integrated waverider with steady state flight
681 constraints. **33rd Aerospace Sciences Meeting and Exhibit**, AIAA Paper 1995-0848, 1995
- 682 [41]. Tian C, Li N, Gong G H, et al. A parameterized geometry design method for inward turning
683 inlet compatible waverider. **Chinese Journal of Aeronautics**, 2013, 26(5): 1135-1146

- 684 [42].Huang H H, Huang G P, Zuo F Y, et al. CFD Simulation of TBCC inlet based on internal
685 waverider concept. **21st AIAA International Space Planes and Hypersonics Technologies**
686 **Conference**, AIAA Paper 2017-2354, 2017
- 687 [43].Xiang X H, Liu Y, Qian Z S. Investigation of a wide range adaptable hypersonic dual-waverider
688 integrative design method based on two different types of 3D inward-turning inlets. **21st AIAA**
689 **International Space Planes and Hypersonics Technologies Conference**, AIAA Paper 2017-
690 2110, 2017
- 691 [44].Wang F M, Ding H H, Lei M F. Aerodynamic characteristics research on wide-speed range
692 waverider configuration. **Science in China Series E: Technological Sciences**, 2009, 52(10):
693 2903-2910
- 694 [45].Li S B, Luo S B, Huang W, et al. Influence of the connection section on the aerodynamic
695 performance of the tandem waverider in a wide-speed range. **Aerospace Science and**
696 **Technology**, 2013, 30: 50-65
- 697 [46].Li S B, Huang W, Wang Z G. Design and aerodynamic investigation of a parallel vehicle on a
698 wide-speed range. **Science China Information Sciences**, 2014, 57(12): 128-201
- 699 [47].Nonweiler T R F. Aerodynamic problems of manned space vehicles. **Journal of the Royal**
700 **Aeronautical Society**, 1959, 63: 521-528
- 701 [48].Gonor A L, Kazakov M N, Shvets A I, et al. Aerodynamic characteristics of star-shaped bodies
702 at supersonic velocities. **Fluid Dynamics**, 1971, 6(1): 86-89
- 703 [49].Gonor A L, Kazakov M N, Shvets A I. Drag measurements on star-shaped body at $M \approx 6$ and
704 8. **Fluid Dynamics**, 1968, 3(1): 64-66
- 705 [50].Reyn J W. Cones of minimum drag in Newtonian flow. **J. Astronaut Sciences**, 1965, 12(2)

- 706 [51].Corda S. Star-body waveriders with multiple design mach numbers. **Journal of Spacecraft**
707 **and Rockets**, 2009, 46(6): 1178-1185
- 708 [52].Zhang T T, Wang Z G, Huang W, Li S B. A design approach of wide-speed-range vehicles
709 based on the cone-derived theory. **Aerospace Science and Technology**, 2017, 71: 42-51
- 710 [53].Li S B, Wang Z G, Huang W, et al. Design and investigation on variable Mach number
711 waverider for a wide-speed range. **Aerospace Science and Technology**, 2018, 76: 291-302
- 712 [54].Zhao Z T, Huang W, Li S B, et al. Variable Mach number design approach for a parallel
713 waverider with a wide-speed range based on the osculating cone theory. **Acta Astronautica**,
714 2018, 147: 163-174
- 715 [55].Liu J, Liu Z, Wen X, et al. Novel osculating flowfield methodology for wide-speed range
716 waverider vehicles across variable Mach number. **Acta Astronautica**, 2019, 162: 160-167
- 717 [56].Ding F, Liu J, Shen C B, et al. An overview of research on waverider design methodology.
718 **Acta Astronautica**, 2017, 140: 190-205
- 719 [57].Purvis J W. Analytical prediction of vortex lift. **17th Aerospace Sciences Meeting**, AIAA Paper
720 79-0363, 1979
- 721 [58].Lee M, Ho C M. Lift force of delta wings. **Applied Mechanics Reviews**, 1990, 43
- 722 [59].Wood R M, Wilcox F J, Steven J, et al. Vortex flows at supersonic speeds. **NASA Center for**
723 **AeroSpace Information**, 2003
- 724 [60].Rodi P E. Vortex lift waverider configurations. **AIAA-2012-1238**, Nashville: AIAA, 2012
- 725 [61].Rodi P E. Geometrical relationships for osculating cones and osculating flowfield waverider.
726 **AIAA-2011-1188**, Orlando: AIAA, 2011
- 727 [62].Duan Y H, Fan Z L, Wu W H. Research on the methods of generation and design of osculation

- 728 cone waverider with constant angle of sweepback. **Acta Aeronautica et Astronautica Sinica**,
729 2016, 37(10): 3023-3034 (in Chinese)
- 730 [63].Liu C Z, Bai P, Chen Y X, et al. Research on the design of the double swept waverider. **21st**
731 **AIAA International Space Planes and Hypersonics Technologies Conference**, AIAA Paper
732 2017-2140, 2017
- 733 [64].Zhao Z T, Huang W, Yan B B, et al. Design and high speed aerodynamic performance analysis
734 of vortex lift waverider with a wide-speed range. **Acta Astronautica**, 2018, 151: 848-863
- 735 [65].Zhao Z T, Huang W, Yan L, et al. Low speed aerodynamic performance analysis of vortex lift
736 waveriders with a wide-speed range. **Acta Astronautica**, 2019, 161: 209-221
- 737 [66].Liu C Z, Liu Q, Bai P, et al. Planform-customized waverider design integrating with vortex
738 effect. **Aerospace Science and Technology**, 2019, 86: 438-443
- 739 [67].Liu C Z, Liu Q, Bai P, et al. Aerodynamic shape design integrating vortex and shock effects
740 for width-velocity-range. **Acta Aeronautica et Astronautica Sinica**, 2018, 39(7): 121824 (in
741 Chinese)
- 742 [68].Wang J F, Liu C Z, Bai P, et al. Design methodology of the waverider with a controllable planar
743 shape. **Acta Astronautica**, 2018, 151: 504-510
- 744 [69].Xu M L, Liu L H, Tang G J, et al. Scheme trajectory design of hypersonic glide-cruise vehicle.
745 **Flight Dynamics**, 2010, 28(5): 51-54 (in Chinese)
- 746 [70].Liu J, Ding F, Huang W, et al. Novel approach for designing a hypersonic gliding-cruising dual
747 waverider vehicle. **Acta Astronautica**, 2014, 102: 81-88
- 748 [71].Wang Q W. The osculating method of the dual waverider geometry generation. **National**
749 **University of Defense Technology**, Changsha, 2015 (in Chinese)

- 750 [72].Liu J, Ding F, Wang Q W, et al. Gliding-cruising two-stage waverider design method based on
751 osculating cone principle. Patent Application Publication, China, 2015, CN 104973266 A
- 752 [73].Liu J, Ding F, Wang Q W, et al. Design method of gliding-and-cruising two-stage waverider
753 based on variable shock wave angles and osculating cone principle. Patent Application
754 Publication, China, 2017, CN 105151316 A
- 755 [74].Liu Z, Liu J, Ding F, et al. Novel methodology for wide-ranged multistage morphing waverider
756 based on conical theory. **Acta Astronautica**, 2017, 140: 362-369
- 757 [75].Liu Z, Liu J, Ding F, et al. Wide-speed-domain multistage variant gliding waverider aircraft
758 designing method based on cone-derived theory. Patent Application Publication, China, 2017,
759 CN 106364697 A
- 760 [76].Weisshaar T A. Morphing aircraft systems: historical perspectives and future challenges.
761 **Journal of Aircraft**, 2013, 50(2): 337-353
- 762 [77].Barbarino S, Bilgen O, Ajaj R M, Friswell M I, Inman D J, et al. A review of morphing aircraft.
763 **Journal of Intelligent Material Systems and Structures**, 2011, 22: 823-877
- 764 [78].Yan B B, Li Y, Dai P, Liu S X, et al. Aerodynamic analysis, dynamic modeling, and control of
765 a morphing aircraft. **Journal of Aerospace Engineering**, 2019, 32(5): 04019058
- 766 [79].Rodriguez A R. Morphing aircraft technology survey. **45th AIAA Aerospace Sciences**
767 **Meeting and Exhibit**, AIAA Paper 2007-1258, 2007
- 768 [80].Bowcutt K G. Hypersonic waverider variable leading edge flaps. Patent Application
769 Publication, USA, 2003, US 6634594 B1
- 770 [81].Maxwell J R. Hypersonic waverider stream surface actuation for variable design point
771 operation. **52nd AIAA/SAE/ASEE Joint Propulsion Conference**, AIAA Paper 2016-4706,

772 2016

773 [82].Phoenix A A, Maxwell J R, Goodwin G B. Morphing high-temperature surfaces for shapeable

774 hypersonic waverider vehicles. **In: Proceedings of the ASME 2017 Conference on Smart**

775 **Materials, Adaptive Structures and Intelligent Systems**, 2017

776 [83].Phoenix A A, Rogers R E, Maxwell J R, et al. Mach five to ten morphing waverider: control

777 point study. **Journal of Aircraft**, 2019, 56(2): 493-504

778 [84].Phoenix A A, Maxwell J R. The Mach 5 to 3.5 morphing waverider optimal actuation location

779 selection. **2018 AIAA/AHS Adaptive Structures Conference**, AIAA Paper 2018-1285, 2018

780 [85].Maxwell J R. Shapeable hypersonic waverider entry vehicles. **53rd AIAA/SAE/ASEE Joint**

781 **Propulsion Conference**, AIAA Paper 2017-4880, 2017

782 [86].Maxwell J R, Goodwin G B. Shapeable inlet manifold for hypersonic scramjet. **55th AIAA**

783 **Aerospace Sciences Meeting**, AIAA Paper 2017-1385, 2017

784 [87].Goodwin G B, Maxwell J R. Performance analysis of a hypersonic scramjet engine with a

785 morphable waverider inlet. **53rd AIAA/SAE/ASEE Joint Propulsion Conference**, AIAA

786 Paper 2017-4651, 2017

787 [88].Maxwell J R. Morphing waveriders for atmospheric entry. University of Maryland College

788 Park, College Park, MD, 2019 (Ph.D.)

789 [89].Takama Y. Practical waverider with outer wings for the improvement of low-speed

790 aerodynamic performance. **17th AIAA International Space Planes and Hypersonic Systems**

791 **and Technologies Conference**, AIAA Paper 2011-2300, 2011

792 [90].Li W D, Ding H H, Wang F M. Research on aerodynamic characteristics of waverider-based

793 vehicles flying at low-Mach states. **Journal of Astronautics**, 2010, 31(5): 1283-1288 (in

794

Chinese)